Assessment of the total precipitable water from a sun-photometer, microwave radiometer and radiosondes at a continental site in southeastern Europe

Konstantinos Fragkos[1], Bogdan Antonescu[1], Dragoş Ene[1], Georgios A. Efstathiou[2], and
Livio Belegante[1]

[1]National Institute of R&D for Optoelectronics INOE 2000, 409 Atomistilor Str., Măgurele, Ilfov, Romania
[2]Department of Mathematics, Centre for Geophysical and Astrophysical Fluid Dynamics, University of Exeter, Exeter, UK

Correspondence: Konstantinos Fragkos (kostas.fragkos@inoe.ro)

Abstract. In this study, we discuss the differences in the total precipitable water (TPW), retrieved from a Cimel sunphotometer operating at a continental site in South-East Europe, between the Version 3 (V3) and Version 2 (V2) of the Aerosol Robotic Network (AERONET) algorithms. In addition, we evaluate the performance of the two algorithms comparing their product with the TPW obtained from a collocated microwave radiometer and nearby radiosondes during the period 2007–2017. The TPW

5   from all three instruments was highly correlated, showing the same annual cycle, with lower values during winter and higher during summer. The Sun-photometer and the microwave radiometer depicts the same daily cycle, with some discrepancies during early morning and late afternoon due to the effect of solar zenith angle on the measurements of the photometer. The TPW from the (V3) of the AERONET algorithm has small differences compared with (V2), mostly related to the use of the new laboratory-based temperature coefficients used in V3. The microwave radiometer shows very good performance compared

10   to the radiosondes, especially during nighttime when the differences between the two instruments are almost negligible. The comparison of the sun-photometer data with high-quality independent measurements from radiosondes and radiometer shows that the absolute differences between V3 and the other two datasets are slightly higher compared with V2. However, V3 has a lower dependence from the TPW and the internal sensor temperature, indicating a better performance of the retrieving algorithm. To our knowledge, this is the first in-depth analysis of the V3 TPW and although the findings presented here are for

15   a specific site, we believe that they are representative of other mid-latitude continental stations.

1   Introduction

Water vapor is a crucial atmospheric component of Earth's climate, since it is the most abundant greenhouse gas IPCC (2013). Water vapor plays a prominent role in the hydrological cycle through water evaporation and condensation while providing the energy to drive moist convection and resulting precipitation. The large-scale flow and local circulations contribute to the large

20   variability of the spatial and temporal distribution of water vapor. For weather forecasting, precipitation efficiency is strongly related to the water vapor content which in turn determines the potential stability of the atmospheric column. Thus, accurate

estimations of water vapor content are essential for meteorological and climate applications such as radiative transfer modeling (e.g., Paynter and Ramaswamy, 2012) or weather forecasting (e.g., Liang et al., 2015).

A common measure of the water vapor content in the atmosphere is the total precipitable water (TPW), defined as the total water "contained in a column of unit cross section extending all of the way from the earth's surface to the top of the

5 atmosphere" (American Meteorological Societycited 2018). Initially, radiosonde measurements have been used to measure TPW (e.g., Reber and Swope, 1972). Although, the radiosonde measurements are reliable they are limited, for example, by freezing of moisture sensors which lead to errors in the estimation of moisture, or by the phase lag between the dry and wet bulb sensors (Campmany et al., 2010). In addition, the global radiosonde network coverage is limited (e.g., McCarthy, 2008). Thus, considering the large variability of water vapor both in time and space, it becomes obvious that soundings provide a very

10 limited spatiotemporal representation of TPW (Liang et al., 2015).

To overcome these issues, a number of methods for TPW estimation based on active or passive remote sensing techniques, either from the ground or the space, have been developed. From the ground the most common ones include the GPS system (Mears et al., 2015), microwave radiometers (Westwater and Guiraud, 1980), Cimel sunphotometers (Halthore et al., 1997; Holben et al., 1998), FTIR (Sussmann et al., 2009) and Raman lidars (Ferrare et al., 1995; Filioglou et al., 2017). Recently,

15 techniques have been developed for the retrieval of TPW from measurements of the precision solar spectroradiometer at World Radiation Center (WRC) Davos (Raptis et al., 2018), the PESR/PREDE-POM sun–sky radiometers (Campanelli et al., 2018) and from Max-DOAS observations (Wagner et al., 2013).

The quality of the retrieved TPW from each instrument is assessed through comparison with other independent measurements. In general, radiosondes and the global GPS systems have been used for the evaluation of TWP measurement from

20 satellite data (Van Malderen et al., 2014; Román et al., 2015; Vaquero-Martínez et al., 2017; Vaquero-Martínez et al., 2017; Gui et al., 2017; Vaquero-Martínez et al., 2018). Of particular interest is the evaluation of the TPW from Cimel sun photometers which are part of AERONET (AErosol RObotic NETwork) a network with global coverage. Several studies have validated the TPW retrieval from Cimel sun-photometers with radiosondes, GPS, and microwave radiometer measurements (Sapucci et al., 2007; Schneider et al., 2010; Campmany et al., 2010; Pérez-Ramírez et al., 2014; Van Malderen et al., 2014; Gui et al., 2017;

25 Campanelli et al., 2018, e.g.,). Although their dense network, Cimel sun-photometers have a series of limitations because they require sun light and clear sky conditions for TPW retrieval. These conditions restrict the availability of data just during daytime and thus reduce the temporal availability of the datasets. Nevertheless, Pérez-Ramírez et al. (2014) demonstrated that Cimel can provide extended time series with good temporal resolution. Lunar photometer could provide TPW during nighttime (e.g., Barreto et al., 2013), but this product is not yet available in the AERONET database.

30 In this article, we focus on measurements conducted at the Romanian Atmospheric 3D Observatory (RADO). The reason for this is that RADO is the only site, to our knowledge, in South-Eastern Europe that has long-term measurements of TPW from three independent instruments (i.e. Cimel sun-photometer, microwave radiometer, radiosondes). Therefore, it can be used as a testbed to assess the quality of the measurements, especially because the radiometer provides continuous, high-quality observations of TPW. Furthermore, this site is one of the few potential sites from South-Eastern Europe that can be used for

35 satellite cal/val activities. Thus, the evaluation of the RADO measurements is an essential process towards this goal.

Recently the newly released version 3 of the AERONET products has become publicly available. This new version incorporates significant improvements for the direct sun measurements, such as a new improved cloud screening algorithm, automated quality check procedures, inclusion of higher airmass data, and new temperature characterization and corrections to all channels (Giles et al., 2016). To our knowledge, no study has evaluated the newly released version of the TPW from the AERONET, so far. In this study, the quality of the TPW measured by three different instruments (i.e., HATPRO-G2 microwave radiometer, a Cimel sun-photometer and radiosondes) at a site in southeastern Europe is assessed. The paper is organized as follows. The instruments used in this study are described in section 2. In section 3, the climatology of the annual cycle of TPW observed over the studies area, and the comparison of the different dataset employed for the measurements of TPW are presented. More specifically the differences between the microwave radiometer and radiosondes, Cimel V2 and V3 and the radiosondes, Cimel V2 and V3 and the radiometer are analyzed and the factors affecting their agreement are assessed. Section 4 summarizes this article.

2 Data and Site description

The HATPRO-G2 microwave radiometer and the Cimel sun-photometer used in this study were located at the Romanian Atmospheric 3D Observatory (RADO,44.82°N, 26.82°E, 93m ASL) part of the National Institute of Research and Development for Optoelectronics (INOE2000). The observatory is located in the city of Măgurele, Ilfov, at the central part of the Romanian plain, approximately 10 km southwest of Bucharest, the capital city of Romania, and is surrounded by research facilities, residence buildings and a small forest. Central Romanian plain has a temperate climate influenced by the western circulation, the east-European anticyclone, the Mediterranean cyclones, and the tropical advections (Cheval et al., 2009).

2.1 Cimel Sun-Photometer

A Cimel Electronique 318A sunphotometer was installed at the RADO facilities in July 2007 and was operated until May 2016, when it was reallocated to Poland. As a replacement a Cimel lunar photometer operates since 2016, but data from this instrument have not been used in this study due to the limited availability of level 2 data. Cimel is the standard instrument of the AERONET (Holben et al., 1998) used to study of the aerosol total column load. It performs spectral measurements of the direct sun irradiance and sky radiance at six discrete wavelengths using interference filters. The filters are centered at the wavelengths of 340, 380, 440, 500, 675, 870, and 1020 nm. An additional channel at 940 nm is used for the retrieval of the TPW. The instrument is calibrated almost annually following the procedures and the guidelines of the AERONET. TPW is calculated based on a modified expression of the Beer-Bouger-Lambert Law. Details about the algorithm can be found in Smirnov et al. (2004) and Schmid et al. (1996). In this study all available data from July 2007 to May 2016, level 2 from the Versions 2 and 3 of AERONET algorithms, were used. Level 2 data are screened for clouds and quality controlled. In addition, the calibration constant of the instrument between two periods has been evaluated. The newest released Version 3 incorporates improvements for the direct sun measurements 1) related to the screening of clouds, 2) the automated data quality assurance, 3) inclusion of data with higher airmasses (i.e., from 1 to 7, in contrast with V2 that ranges from 1 to 5), 4) implementation of

spectral temperature corrections based on laboratory measurements (i.e., unlike Version 2 that was based on the manufacture specifications) (Giles et al., 2016). Pérez-Ramírez et al. (2014) evaluated the TPW from AERONET at the U.S. Department of Energy Atmospheric Radiation Measurement Program (ARM) sites against microwave radiometers, GPS, and radiosondes, and concluded that Cimel has a maximum overall uncertainty of less than 15%.

2.2 Microwave radiometer

The HATPRO-G2 microwave radiometer used in this study was produced by Radiometer Physics GmbH. It is a passive instrument working in the microwaves regime. It consists of two working bands 22–31 GHz and 51–58 GHz, each with 7 channels. The relevant receiving optics, the ambient load, the internal scanning mechanism, the electronics and the data acquisition system of the radiometer are described in Rose et al. (2005). For humidity profiling only the first band is used. The vertical resolution for profiling is variable, ranging from 200 meters bellow 2000 m to 800 m for altitudes higher than 5000 m. In this study, the integrated water vapor (IWV) was used, which presents, according to the manufacturer[1], an accuracy of ± 0.2 kg m^{-2} RMS and noise of 0.05 kg m^{-2}. Considering the density of liquid water, the IWV expressed in kg m^{-2} is equivalent with the TPW expressed in mm of liquid water (Bevis et al., 1992). In this study measurements are performed each 2 seconds. To ensure the high quality of measurements, the instrument is absolutely calibrated with liquid nitrogen every 6 months following the instructions of the manufacturer. All the available data between 16 December 2009 and 31 December 2017 were used. Data which have been flagged as rain from the internal sensor of the instrument have been removed. In addition, the data have been visually inspected to remove all the points associated with instrument malfunction that were not captured by the internal quality control of the instrument.

2.3 Radiosondes

The radiosonde measurements were obtained from the sounding database maintained by the University of Wyoming[2]. Between July 2007 and December 2017, 3760 radiosonde measurements for 0000 UTC and 3759 for 1200 UTC were available from the Bucharest site, situated at approximately 30 km northeast from the RADO facility, and operated by the Romanian National Meteorological Administration. The radiosondes used during the study period were Vaisala RS92 type. For this type of radiosondes, Miloshevich et al. (2009) showed that the accuracy of the humidity sensor during daytime depends on the calibration error and the dry bias due to the solar heating effect (Turner et al., 2003) and during the nighttime just from the calibration error.The overall uncertainty of TPW from radiosonde measurements have been estimated to $\pm 5\%$ (Pérez-Ramírez et al., 2014). TPW over the entire sounding was calculated as

$$TPW = \frac{1}{\rho g} \int_{p_1}^{p_2} x \, dp \tag{1}$$

---

[1]RPG-HATPRO-G4 series Microwave radiometers for continuous atmospheric profiling, access from https://www.radiometer-physics.de/download/PDF/Radiometers/HATPRO/RPG_MWR_PRO_TN.pdf on 13 July 2018.

[2] http://weather.uwyo.edu/upperair/sounding.html, access on 13 July 2018.

were $x(p)$ is the mixing ration at the pressure level p, ρ is the density of water and g is the acceleration of gravity.

3   Results

3.1   Climatology of total precipitable water in Măgurele

For the computation of the daily mean values of TPW all available measurements were used. Table 1 gives an overview of the
total number of observations that have been analyzed along with their total number of corresponding days. The times series
of the daily mean values for the TPW from the different instruments employed in this study are shown in Fig. 1. In general,
the radiosonde measurements are available twice per day (i.e., 0000 and 1200 UTC). The Cimel measurements are restricted
only during day time and under clear sky conditions, while the microwave radiometer performs measurements during day and
night time under all weather conditions. Although there are differences in measurements schedule, all three instruments depict
the same annual cycle, demonstrating their capability of performing long-term measurements for climatological applications
(Fig. 1). The gaps in the radiometer time-series are due to instrumental related issues and the ones in Cimel time series due to
the calibration of the instrument which requires the reallocation of the instrument. Data gaps of the microwave radiometer are
due to malfunction of the instrument or controlling PC (usually solved with a restart after a maximum of couple of days), or
due to the relocation of the instrument during different measurement campaigns (data not included in this study). Furthermore,
in the beginning of 2016 the instrument was sent to the manufacturer for testing and replacing several components.

The observed differences in the mean values calculated from all instruments (Table 2), are mostly due to the different
operating period of each instrument and their different sampling rate. The minimum daily values can be as low as 2 mm, while
the maximum exceed 44 mm (Table 2). The peak-to-peak range during the year (i.e., from minimum to maximum) can be up
to 20 mm.

The annual cycle of the TPW as depicted by all three instruments, has minimum during winter months (DJF) and a maximum
during summer months (JJA) (Fig. 2). Higher air temperature during the summer implies a larger capacity to store water vapor
without saturation (Campmany et al., 2010). The small differences on the monthly median values for all instruments are due
to their different sampling rates. For example, the increased number of outliers in the radiosondes boxplots, compared to the
other instruments, can be attributed to the limited number of measurements (i.e., a maximum of two per day). Thus, some
high/low values are not smoothed by averaging all measurements during the day (Fig. 2a). In any case, the main aim of the
analysis presented here is to show that the annual cycle of TPW can be depicted fairly well by all instruments and demonstrate
their capabilities for long-term monitoring for climatological applications. A direct comparison of the daily values from each
instrument would not be valid due to the very different sampling rates and the diurnal variation of TWP as shown in Fig. 3. An
overview of the statistical values for all three instruments is shown in Table 3.

3.2 Sensitivity of the instruments to diurnal variation

As mentioned previously, the temporal resolution of the microwave radiometer is on order of few seconds in combination with its capacity to operate under all weather conditions allow the detection of the TWP diurnal variations. In addition, under clear sky conditions, the Cimel sun-photometer perform measurements at about every 20 min. To verify if both instruments

5   depict the same daily cycle, the diurnal variability for six randomly selected days was examined. The days were selected under the condition that the number of Cimel observations was enough so as the daily cycle can be captured, indicating that there were clear or near clear sky conditions. Cimel and the microwave radiometer depict the same diurnal variation during daytime (Fig. 3), with some small differences in their absolute values which are further investigated in the following sections. For some of the selected days (i.e., 08 June 2012, 26 October 2013) there are differences in the diurnal variation during the early morning

10   or late afternoon hours, which are most likely artifacts associated with direct sun measurements at high aimasses.

3.3 Comparison between radiosondes and radiometer

To account for spatial and temporal differences between the radiosonde and the microwave radiometer, all the microwave radiometer data were averaged over an interval of 20 min centered on the radiosonde launching time. A total number of 2789 common measurements, out of which 1400 during daytime (i.e., at 1200 UTC) and 1389 during night (i.e., at 0000 UTC) were

15   extracted for the comparison. The absolute and relative differences between two sets of measurements were defined as

$$X - X_{ref} \tag{2}$$

and

$$100 \cdot \frac{(X - X_{ref})}{X_{ref}} \tag{3}$$

respectively, where (X_{ref}) is the reference measurement (i.e., the radiosonde measurement, except for the comparison between

20   Cimel and the microwave radiometer).

The relative difference between the two datasets is in general between $\pm 25\%$ (Fig. 4). The radiosondes slightly underestimate TPW with the overall difference from the microwave radiometer to be $1.80 \pm 9.72\%$ (0.17 ± 1.66 mm). This underestimation is more evident during daytime (i.e., $3.13 \pm 10.06\%$ or 0.34 ± 1.72 mm) due to the known dry bias effect, while during nighttime the differences are almost negligible (i.e., $0.45 \pm 9.17\%$ or 0.005 ± 1.584 mm).

25   The two datasets are highly correlated (Fig. 5a; $R^2 = 0.97$), with the majority of the points to be over the $y = x$ line. However, for the higher values of TPW (i.e., TPW>30 mm) an increased scatter of the data is observed, without being significant high. The histogram of the relative differences between the two instruments approximates a normal distribution, peaking at about 1% (Fig. 5b). About 96% of the data are between $\pm 20\%$, while $\sim 78\%$ lie in the range $\pm 10\%$. The difference between the two datasets has a small dependence from the TPW amount of -0.171% mm^{-1} (Fig. 6a). This dependence is more evident

30   for the daytime measurements (i.e., for radiosondes launched at 1200 UTC; Fig. 6b), while for the nighttime measurements the dependence is almost negligible (i.e., $-0.088 \pm 0.052\%$ mm^{-1}; Fig. 6c). The best agreement between the two datasets is

achieved for TPW values ranging between 15 and 35 mm. The increased difference for TPW values higher than 40 mm cannot be fully evaluated due to the very small number of observations.

3.4 Comparison of Cimel V2 and V3

To assess the differences of the TPW derived from the newly released Version 3 from AERONET and the previous Version 2,
5   their common measurements were used. The difference in the number of observations between the two Versions (see Table 1) arises from the fact that they have different quality control and cloud screening procedures (Giles et al., 2016). A total number of 27707 common observations between the two Versions were extracted for comparison. In general, the differences between the two Versions are small, ranging in general between $\pm 2\%$ and rarely exceed 5%, with V2 having higher values than V3 (Fig. 7). The overall difference between the two datasets for the period 2007–2016 is $0.60\pm 20.91\%$ (0.08 ± 20.14 mm). The
10   largest differences occur in periods after the calibration, while some others may be due to the degradation of the filters because of aging and temperature effects, associated with the different way that the temperature coefficients are calculated.

    To further evaluate the differences between TPW from the two different Versions of the AERONET algorithm, a series of factors that could affect the measurements (i.e., the total amount of TPW, the SZA, the sensor temperature) were examined. No dependence was found with the SZA. The relative difference between V2 and V3 shows a dependence from TPW (Fig. 8a).
15   The biggest differences (i.e., $\sim 2.5\%$) are observed for TPW values lower than 10 mm, while the agreement between the two datasets improves with increased TPW values. However, the decrease in the relative difference of TPW between V2 and V3 is due to the different treatment of the temperature correction in the versions. As shown in Fig. 2 the lowest TPW values appear during wintertime, when the temperature is low as well. Corresponding to these low temperature values the differences between V2 and V3 shows maximum value of $\sim 2.5\%$ (Fig. 8b). A very pronounced dependence is also seen by the temperature
20   of the internal sensor of the instrument. This dependence is due to the different temperature coefficients in the two versions of the retrieval algorithm. For V2 the temperature coefficients are based on the manufacturer specifications, while in V3 the temperature characterization is based on laboratory measurements during the calibration of the instrument. The highest positive differences, the order of $\sim 2.5\%$ appear for low temperatures ($<10^\circ$C). For the whole range of temperatures that are recorded in the instrument (i.e., $\sim 50^\circ$C) a total difference of up to 2.5% is observed (Fig. 8b).

25 ## 3.5 Comparison between Cimel and radiosondes

To have a better overview about how the differences between the two versions affect the agreement with the other instruments, the evaluation of Cimel measurements with radiosondes and microwave radiometer was based on the common dataset between the two different algorithm version (section 3.4). Because Cimel does not measure during nighttime and the comparison is limited to daytime measurements only (i.e., radiosondes launched at 1200 UTC). To account for spatial and temporal differences,
30   the same procedure with the one described for the comparison between microwave radiometer and radiosondes was used (i.e., averaging all Cimel points over an interval of 20 min centered on the radiosonde launching time). Thus, a total number of 565 common measurements were identified.

The differences between Cimel and radiosondes range between ±20% Fig. 9, while the overall mean difference is -2.04±10.62% (or -0.37±2.05 mm) and –2.81±10.23% (or -0.48±1.97 mm), for V2 and V3 respectively. These results are in agreement with previous studies which showed that AERONET sun-photometers generally underestimate TPW in comparison with other in-struments (Campmany et al., 2010; Pérez-Ramírez et al., 2014; Gui et al., 2017; Campanelli et al., 2018). The Version 3 shows an increased underestimation of TPW in comparison with the radiosondes, however the standard deviation is slightly better than the previous version (Fig. 9b).

The TPW from both versions is highly correlated with the TPW from the radiosondes (i.e., the correlation coefficient is 0.974 and 0.976 for CV2 and CV3, respectively; (Fig. 10a and Fig. 10c), with the slope of the least square regression line to be very close to unity. The histogram of the relative differences between the two datasets approximates a normal distribution, having a very small kurtosis towards negative values, for both CV2 and CV3 (Figs. 10b and d). For CV2 about 65% of the differences are between ±10%, while ∼93% are between ±20%. For CV3 the respective numbers are 67% and 93%. The low number of the coincidence measurements, and their big scatter among different SZAs, TPWs and temperatures of the sensor, do allow a further evaluation of the influences from these factors.

3.6 Comparison between Cimel and Radiometer

The comparison between Cimel and microwave radiometer is based on their coincidence measurements, with the microwave radiometer observations averaged over a 1-min interval. This common dataset consists of 8505 observations for the period December 2009–May 2016. The differences between the TPW from both versions of AERONET algorithms are in generally between ±10% Fig. 11. Cimel underestimates the TPW by 2.75±5.85% (or 0.70±1.22 mm) and 3.57±5.54% (or 0.81±1.17 mm), for V2 and V3, respectively. Some periods with increased underestimation (i.e., mid 2012) may be due to calibration issues, because after the Cimel calibration (i.e., at the beginning of 2013) the observed degradation stopped.

The TPW from Cimel (both CV2 and CV3) and microwave radiometer are highly correlated (Figs. 12a and c; R = 0.993). Taking into consideration that the microwave radiometer and the Cimel have the same diurnal variations (section 3.2) a very high correlation of the two datasets was expected. For higher values of TPW there is a deviation from the identity line.

The histogram of the relative differences between the two datasets approximates a normal distribution, having a very small flattening towards negative values, for both CV2 and CV3 (Figs. 12b and d). For CV2 about 88% of the differences lie between ±10%, while almost the entirely dataset is between ±20% (>99%). For CV3 the respective values are similar. These results show a very good agreement between the two different methods for the retrieval of TPW.

The difference of the TPW between the Cimel and the microwave radiometer do now show a pronounced dependence from the SZA (Figs. 13a and b), for both versions of AERONET algorithms. However, there is an increased scatter for SZAs higher than 70°. We speculate that this is due to the increased stray-light that can affect the direct sun measurements from the Cimel sun-photometer, resulting in an increased uncertainty on the retrieved TPW.

The difference of the TPW between Cimel and microwave radiometer has a small dependence with the total amount of TPW of -1.97% per 10 mm for CV2 and -1.38% per 10 mm for CV3 (Figs. 13c and d). The lower dependence of TPW from CV3 from the total amount of TPW in comparison with CV2 is an indication that the changes applied in the newer version of the

algorithm is towards the right direction. Both versions show a higher variability for TPW values lower than 10 mm. However, this variability is based on a relative low number of observations and is highly affected from some outliers observed (i.e., differences higher >20%) for extremely low TPW values (i.e., 1.5–2 mm). In addition the very low variability for TPW values higher than 40 mm cannot be evaluated because is based on a very limited number of observations (i.e., six observations).

5   The new laboratory based temperature coefficients for the sun-photometer filters, improve the quality of the retrieved TPW from Cimel, as it can be depicted from the comparison with the MWV (Fig. 13f). The dependence of the difference between CV3 and the MWV from the temperature recorded in the sensor of the Cimel photometer, is substantially improved in comparison with the one of CV2 (the order of -0.61% per 10°C and -1.07% per 10°C, for CV3 and CV2, respectively; Fig. 13e and f). Thus the corrections from the application of the new temperature coefficients are important, since they significantly improve

10   the quality of the retrieved TPW for all the operating temperatures.

4   Conclusions

In this study different measurements techniques for TWP (e.g., radiosonde, microwave radiometer, Cimel sun-photometer) were compared over a period of nine years. The microwave radiometer and Cimel sun-photometer operated at the RADO observatory situated at a distance of approximately 10 km from the Bucharest city center. The radiosondes measurements were

15   provided by the Romanian National Meteorological Administration, approximately 18 km from the RADO facilities. The main conclusions of this study can be summarized as follow:

– All three instruments depict the same annual cycle of TPW despite their different sampling rates. Some small differences observed in the monthly mean values can be attributed to the different schedule (i.e., microwave radiometer operates both during daytime and nighttime, while Cimel only during daytime and under clear sky conditions) and their different

20   sample, partly due to the existing gaps in MWV and Cimel.

– The measurements of the microwave radiometer are highly correlated with those from radiosondes (i.e., R = 0.98), indicating that the microwave radiometer can capture the environmental changes that lead to variations in TPW.

– Compared with the microwave radiometer the radiosondes slightly underestimates the TPW especially during daytime measurements (i.e., 3.13±10.06% or 0.34±1.74 mm) due to the dry bias effect, while the difference between the two

25   datasets during nighttime is almost negligible (i.e., 0.45±9.17% or 0.0005±1.58 mm). In addition, the differences between the two datasets during nighttime show a very small dependence (i.e., -0.088±0.052 mm^{-1}) from the total TPW amount, in conjunction with the daytime that have an increased dependency (i.e., -0.250±0.058 mm^{-1}).

– Version 3 of the AERONET algorithm slightly underestimates TPW, compared to Version 2.

– The differences of the TPW between the Versions 2 and 3 AERONET algorithms are small (i.e.,±2%). The highest

30   differences are observed for low temperatures of the internal sensor (i.e.,<10°C), while the use of new laboratory based

temperature coefficients has an effect of up to 2.5% for the whole range of the temperatures recorded by the instrument
($\sim$50°C).

– TPW from Cimel is highly correlated with the radiosonde measurements (i.e., R$>$0.97) for both versions of the AERONET
algorithm.

– Comparison with the radiosondes, Cimel underestimates the TPW by 2.04$\pm$10.62% (or 0.37$\pm$2.05 mm) for V2 and
2.81$\pm$10.23% (or 0.48$\pm$1.97 mm) for V3 respectively. This underestimation is in agreement with previous studies comparing measurement from radiosondes and sun-photometers for different regions.

– When compared with the microwave radiometer, Cimel underestimates by 2.75$\pm$5.85% (or 0.70$\pm$1.22 mm) for V2 and
3.57$\pm$5.54% (or 0.81$\pm$1.17 mm) for V2. The two instruments have the same daily cycle, which shows the capability
of Cimel to capture the daily variations in TPW. However, some discrepancies are observed during early morning or
late afternoon, which can be attributed to the SZA effect. While the difference Cimel and radiometer does not show
any pronounced dependence from SZA, for SZAs $>$70° the differences show an increased scatter. The V3 has a lower
dependence from the total TPW amount (i.e., -0.138$\pm$0.012 mm^{-1} compared with V2 (i.e., -0.197$\pm$0.013 mm^{-1}). The
new laboratory based temperature coefficients implemented in V3 reduced the dependence of the recorded differences
between Cimel and microwave radiometer (i.e., -0.107$\pm$0.012 °C^{-1} and -0.061$\pm$0.011 °C^{-1}, for V2 and V3 respectively).

To our knowledge this is the first study to evaluate in depth the TPW from the newly released Version 3 of the Aeronet
algorithm. The comparison with high quality independent measurements from radiosondes and a collocated radiometer shows
that the absolute level of the differences in V3 from the other instruments is a little higher than in V2. However, V3 has
a lower dependence from the TPW and the internal sensor temperature, indicating an improvement of the product. Further
evaluation for sites with different characteristics is required. Although these findings are for a specific site, they are likely
representative for other continental sites as well. A future study will investigate the accuracy of the nighttime TPW from Cimel
lunar measurements, available at the RADO facilities since 2016, following the methodology applied in this study. Finally, the
microwave radiometer shows a very good performance compared with the radiosondes, especially during nighttime when the
differences between the two instruments are almost negligible. Thus, the microwave radiometer can be used in future studies
related to the validation of satellite datasets both during day and night time.

Data availability. The data from the radiosondes for Bucharest (station id: 15420) are publicly available through the upper air observations
database of the University of Wyoming at the link: http://weather.uwyo.edu/upperair/sounding.html. The Cimel sun-photometer data can be
found at the AERONET website (https://aeronet.gsfc.nasa.gov/) under the site: Bucharest_Inoe. The data from the microwave radiometer are
available upon request.

Acknowledgements. This work has received funding from the European Union's Horizon 2020 Research and Innovation Programme, under grant agreement no. 692014, project ECARS (East European Centre for Atmospheric Remote Sensing), and G.A. 654109 - ACTRIS 2, and the Romanian Ministry of Research and Innovation throughout the Core National Program, Proj. No. 33N/16.03.2018.

References

American Meteorological Society: Precipitable Water. Glossary of Meteorology, [Available online at http://http://glossary.ametsoc.org/wiki/ Precipitable_water], cited 2018.

Barreto, A., Cuevas, E., Damiri, B., Romero, P. M., and Almansa, F.: Column water vapor determination in night period with a lunar photometer prototype, Atmospheric Measurement Techniques, 6, 2159–2167, https://doi.org/10.5194/amt-6-2159-2013, 2013.

Bevis, M., Businger, S., Herring, T. A., Rocken, C., Anthes, R. A., and Ware, R. H.: GPS meteorology: Remote sensing of atmospheric water vapor using the global positioning system, Journal of Geophysical Research: Atmospheres, 97, 15 787–15 801, https://doi.org/10.1029/92JD01517, https://agupubs.onlinelibrary.wiley.com/doi/abs/10.1029/92JD01517, 1992.

Campanelli, M., Mascitelli, A., Sanò, P., Diémoz, H., Estellés, V., Federico, S., Iannarelli, A. M., Fratarcangeli, F., Mazzoni, A., Realini, E., Crespi, M., Bock, O., Martínez-Lozano, J. A., and Dietrich, S.: Precipitable water vapour content from ESR/SKYNET sun–sky radiometers: validation against GNSS/GPS and AERONET over three different sites in Europe, Atmospheric Measurement Techniques, 11, 81–94, https://doi.org/10.5194/amt-11-81-2018, 2018.

Campmany, E., Bech, J., Rodríguez-Marcos, J., Sola, Y., and Lorente, J.: A comparison of total precipitable water measurements from radiosonde and sunphotometers, Atmospheric Research, 97, 385–392, https://doi.org/10.1016/j.atmosres.2010.04.016, 2010.

Cheval, S., Dumitrescu, A., and Bell, A.: Spatial sampling requirements for monitoring upper-air climate change with radiosondes, Theor. Appl. Climatol., 97, 391–401, https://doi.org/10.1007/s00704-008-0088-3, 2009.

Ferrare, R. A., Melfi, S. H., Whiteman, D. N., Evans, K. D., Schmidlin, F. J., and Starr, D. O.: A Comparison of Water Vapor Measurements Made by Raman Lidar and Radiosondes, Journal of Atmospheric and Oceanic Technology, 12, 1177–1195, https://doi.org/10.1175/1520-0426(1995)012<1177:ACOWVM>2.0.CO;2, 1995.

Filioglou, M., Nikandrova, A., Niemelä, S., Baars, H., Mielonen, T., Leskinen, A., Brus, D., Romakkaniemi, S., Giannakaki, E., and Komppula, M.: Profiling water vapor mixing ratios in Finland by means of a Raman lidar, a satellite and a model, Atmospheric Measurement Techniques, 10, 4303–4316, https://doi.org/10.5194/amt-10-4303-2017, 2017.

Giles, D., Holben, B., Smirnov, A., Eck, T., Slutsker, I., Sorokin, M., Schafer, J., and Sinyuk, A.: Evaluation of AERONET AOD Measurements in the Version 3 Database, in: Lidar Data and its use in Model Verification and Data Assimilation, https://aeronet.gsfc.nasa.gov/new_web/Documents/AERONET_V3_AOD.pdf, July 12–14, 2016, College Park, MD, USA, 2016.

Gui, K., Che, H., Chen, Q., Zeng, Z., Liu, H., Wang, Y., Zheng, Y., Sun, T., Liao, T., Wang, H., and Zhang, X.: Evaluation of radiosonde, MODIS-NIR-Clear, and AERONET precipitable water vapor using IGS ground-based GPS measurements over China, Atmospheric Research, 197, 461–473, https://doi.org/https://doi.org/10.1016/j.atmosres.2017.07.021, 2017.

Halthore, R. N., Eck, T. F., Holben, B. N., and Markham, B. L.: Sun photometric measurements of atmospheric water vapor column abundance in the 940-nm band, Journal of Geophysical Research: Atmospheres, 102, 4343–4352, https://doi.org/10.1029/96JD03247, 1997.

Holben, B. N., Eck, T. F., Slutsker, I., Tanré, D., Buis, J. P., Setzer, A., Vermote, E., Reagan, J. A., Kaufman, Y. J., Nakajima, T., Lavenu, F., Jankowiak, I., and Smirnov, A.: AERONET—A Federated Instrument Network and Data Archive for Aerosol Characterization, Remote Sensing of Environment, 66, 1–16, https://doi.org/https://doi.org/10.1016/S0034-4257(98)00031-5, 1998.

IPCC: Summary for Policymakers, in: Climate Change 2013 - The Physical Science Basis, edited by Intergovernmental Panel on Climate Change, pp. 1–30, Cambridge University Press, Cambridge, https://doi.org/10.1017/CBO9781107415324.004, https://www.cambridge.org/core/product/identifier/CBO9781107415324A009/type/book{_}part, 2013.

Liang, H., Cao, Y., Wan, X., Xu, Z., Wang, H., and Hu, H.: Meteorological applications of precipitable water vapor measurements retrieved by the national GNSS network of China, Geodesy and Geodynamics, 6, 135–142, https://doi.org/10.1016/J.GEOG.2015.03.001, 2015.

McCarthy, M. P.: Spatial sampling requirements for monitoring upper-air climate change with radiosondes, Int. J. Climatol., 28, 985–993, https://doi.org/10.1002/joc.1611, 2008.

5 Mears, C. A., Wang, J., Smith, D., and Wentz, F. J.: Intercomparison of total precipitable water measurements made by satellite-borne microwave radiometers and ground-based GPS instruments, Journal of Geophysical Research: Atmospheres, 120, 2492–2504, https://doi.org/10.1002/2014JD022694, 2015.

Miloshevich, L. M., Vömel, H., Whiteman, D., and Leblanc, T.: Accuracy assessment and correction of Vaisala RS92 radiosonde water vapor measurements, Journal of Geophysical Research: Atmospheres, 114, https://doi.org/10.1029/2008JD011565, 2009.

10 Paynter, D. and Ramaswamy, V.: Variations in water vapor continuum radiative transfer with atmospheric conditions, J. Geophys. Res., p. D16310, https://doi.org/10.1029/2012JD017504, 2012.

Pérez-Ramírez, D., Whiteman, D. N., Smirnov, A., Lyamani, H., Holben, B. N., Pinker, R., Andrade, M., and Alados-Arboledas, L.: Evaluation of AERONET precipitable water vapor versus microwave radiometry, GPS, and radiosondes at ARM sites, Journal of Geophysical Research: Atmospheres, 119, 9596–9613, https://doi.org/10.1002/2014JD021730, 2014.

15 Raptis, P.-I., Kazadzis, S., Gröbner, J., Kouremeti, N., Doppler, L., Becker, R., and Helmis, C.: Water vapour retrieval using the Precision Solar Spectroradiometer, Atmospheric Measurement Techniques, 11, 1143–1157, https://doi.org/10.5194/amt-11-1143-2018, 2018.

Reber, E. E. and Swope, J. R.: On the Correlation of the Total Precipitable Water in a Vertical Column and Absolute Humidity at the Surface, Journal of Applied Meteorology, 11, 1322–1325, https://doi.org/10.1175/1520-0450(1972)011<1322:OTCOTT>2.0.CO;2, 1972.

Román, R., Antón, M., Cachorro, V., Loyola, D., Ortiz de Galisteo, J., de Frutos, A., and Romero-Campos, P.: Comparison of total water
20 vapor column from GOME-2 on MetOp-A against ground-based GPS measurements at the Iberian Peninsula, Science of The Total Environment, 533, 317–328, https://doi.org/10.1016/J.SCITOTENV.2015.06.124, 2015.

Rose, T., Crewell, S., Löhnert, U., and Simmer, C.: A network suitable microwave radiometer for operational monitoring of the cloudy atmosphere, Atmospheric Research, 75, 183–200, https://doi.org/https://doi.org/10.1016/j.atmosres.2004.12.005, 2005.

Sapucci, L. F., Machado, L. A. T., Monico, J. F. G., and Plana-Fattori, A.: Intercomparison of Integrated Water Vapor Es-
25 timates from Multisensors in the Amazonian Region, Journal of Atmospheric and Oceanic Technology, 24, 1880–1894, https://doi.org/10.1175/JTECH2090.1, 2007.

Schmid, B., Thorne, K. J., Demoulin, P., Peter, R., Mätzler, C., and Sekler, J.: Comparison of modeled and empirical approaches for retrieving columnar water vapor from solar transmittance measurements in the 0.94-μm region, Journal of Geophysical Research: Atmospheres, 101, 9345–9358, https://doi.org/10.1029/96JD00337, 1996.

30 Schneider, M., Romero, P. M., Hase, F., Blumenstock, T., Cuevas, E., and Ramos, R.: Continuous quality assessment of atmospheric water vapour measurement techniques: FTIR, Cimel, MFRSR, GPS, and Vaisala RS92, Atmospheric Measurement Techniques, 3, 323–338, https://doi.org/10.5194/amt-3-323-2010, 2010.

Smirnov, A., Holben, B. N., Lyapustin, A., Slutsker, I., and Eck, T. F.: AERONET Processing Algorithms Refinement: Proceedings of AERONET Workshop, El Arenosillo, NASA/GSFC Aeronet Project, Spain, 2004.

35 Sussmann, R., Borsdorff, T., Rettinger, M., Camy-Peyret, C., Demoulin, P., Duchatelet, P., Mahieu, E., and Servais, C.: Technical Note: Harmonized retrieval of column-integrated atmospheric water vapor from the FTIR network – first examples for long-term records and station trends, Atmospheric Chemistry and Physics, 9, 8987–8999, https://doi.org/10.5194/acp-9-8987-2009, 2009.

Turner, D. D., Lesht, B. M., Clough, S. A., Liljegren, J. C., Revercomb, H. E., and Tobin, D. C.: Dry Bias and Variability in Vaisala RS80-H Radiosondes: The ARM Experience, Journal of Atmospheric and Oceanic Technology, 20, 117–132, https://doi.org/10.1175/1520-0426(2003)020<0117:DBAVIV>2.0.CO;2, 2003.

Van Malderen, R., Brenot, H., Pottiaux, E., Beirle, S., Hermans, C., De Mazière, M., Wagner, T., De Backer, H., and Bruyninx, C.: A
5 multi-site intercomparison of integrated water vapour observations for climate change analysis, Atmospheric Measurement Techniques, 7, 2487–2512, https://doi.org/10.5194/amt-7-2487-2014, 2014.

Vaquero-Martínez, J., Antón, M., Ortiz de Galisteo, J. P., Cachorro, V. E., Costa, M. J., Román, R., and Bennouna, Y. S.: Validation of MODIS integrated water vapor product against reference GPS data at the Iberian Peninsula, International Journal of Applied Earth Observation and Geoinformation, 63, 214–221, https://doi.org/10.1016/J.JAG.2017.07.008, 2017.

10 Vaquero-Martínez, J., Antón, M., Ortiz de Galisteo, J. P., Cachorro, V. E., Álvarez-Zapatero, P., Román, R., Loyola, D., Costa, M. J., Wang, H., Abad, G. G., and Noël, S.: Inter-comparison of integrated water vapor from satellite instruments using reference GPS data at the Iberian Peninsula, Remote Sensing of Environment, 204, 729–740, https://doi.org/10.1016/J.RSE.2017.09.028, 2018.

Vaquero-Martínez, J., Antón, M., de Galisteo, J. P. O., Cachorro, V. E., Wang, H., Abad, G. G., Román, R., and Costa, M. J.: Validation of integrated water vapor from OMI satellite instrument against reference GPS data at the Iberian Peninsula, Science of The Total Environment,
15 580, 857–864, https://doi.org/10.1016/J.SCITOTENV.2016.12.032, 2017.

Wagner, T., Andreae, M. O., Beirle, S., Dörner, S., Mies, K., and Shaiganfar, R.: MAX-DOAS observations of the total atmospheric water vapour column and comparison with independent observations, Atmospheric Measurement Techniques, 6, 131–149, https://doi.org/10.5194/amt-6-131-2013, 2013.

Westwater, E. R. and Guiraud, F. O.: Ground-based microwave radiometric retrieval of precipitable water vapor in the presence of clouds
20 with high liquid content, Radio Science, 15, 947–957, https://doi.org/10.1029/RS015i005p00947, 1980.
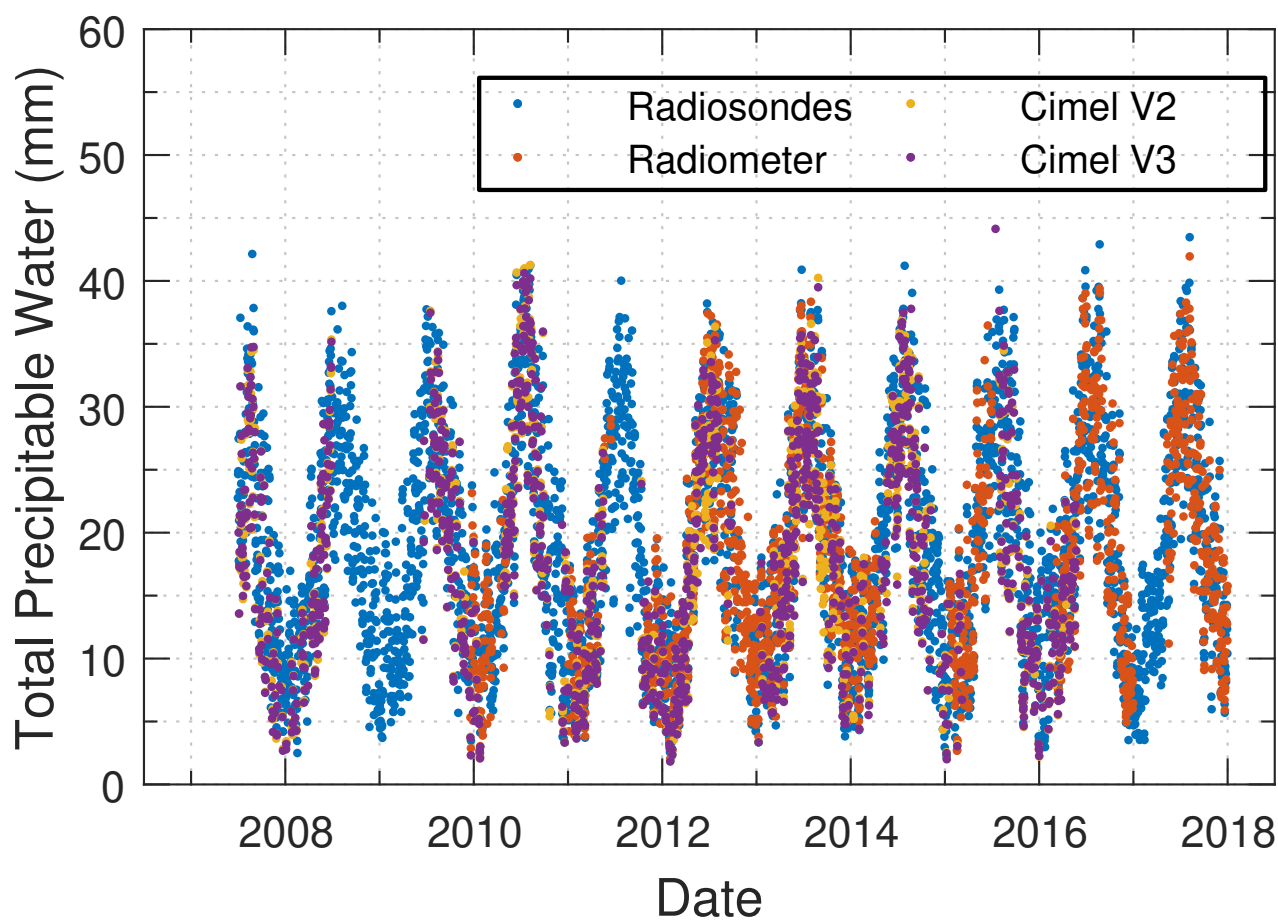
Figure 1. Time series of the daily mean values of the total precipitable water during the period 2007–2017 based on measurements from radiosondes (blue dots), microwave radiometer (orange dots), and Cimel sun-photometer Version 2 (yellow dots) and Version 3 (magenta dots) of the algorithm.
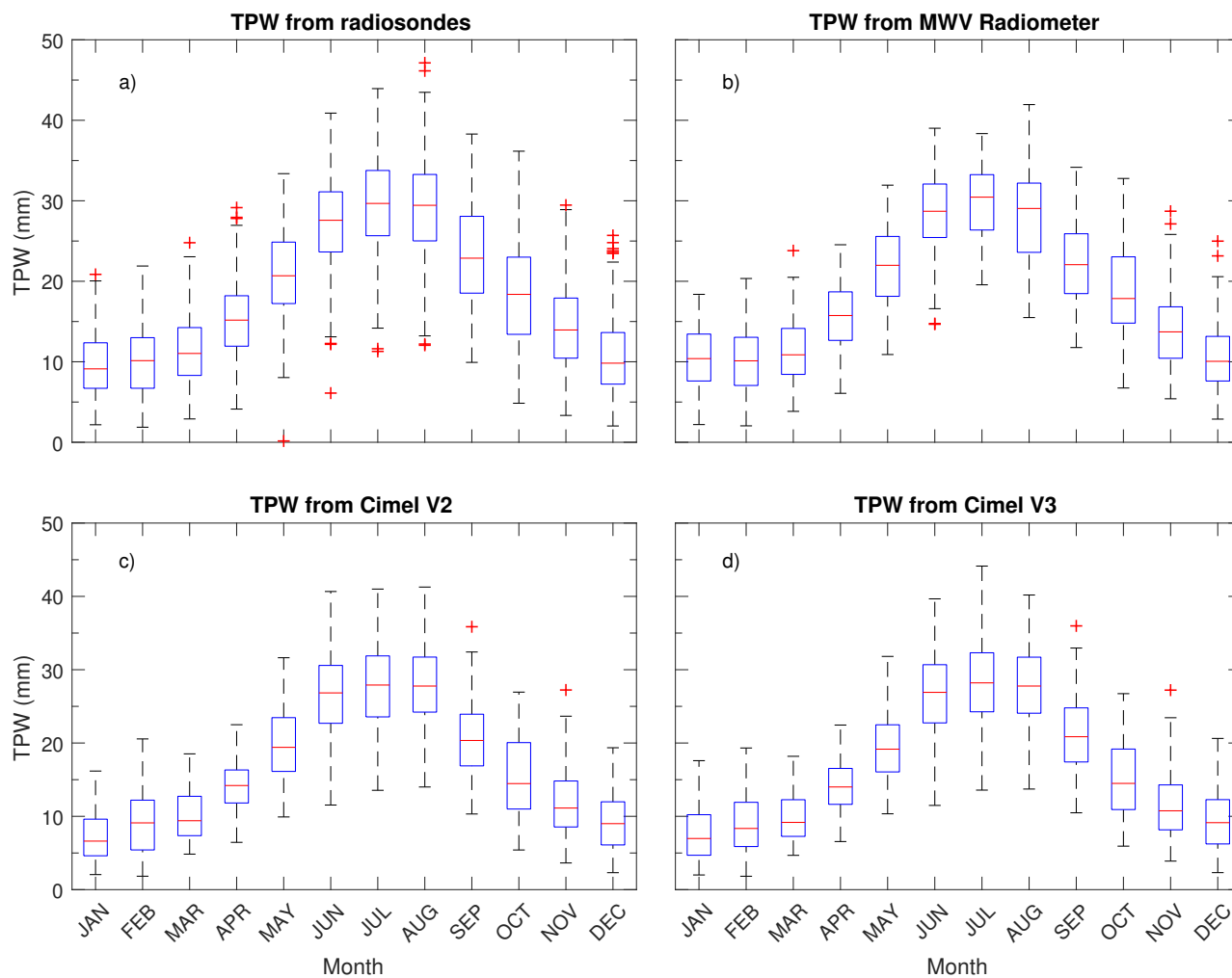
Figure 2. Monthly variation of total precipitable water from a) radiosondes during the period 2007—2017, b) microwave radiometer during the period 2009—2017, c) Cimel sun-photometer version 2 data, and d) cimel sun-photometer version 3 data for the period 2007—2016. The median value are shown as the red lines, the interquartile range (IQR) is spanned by the vertical bars and the whiskers show the 1.5IQR.
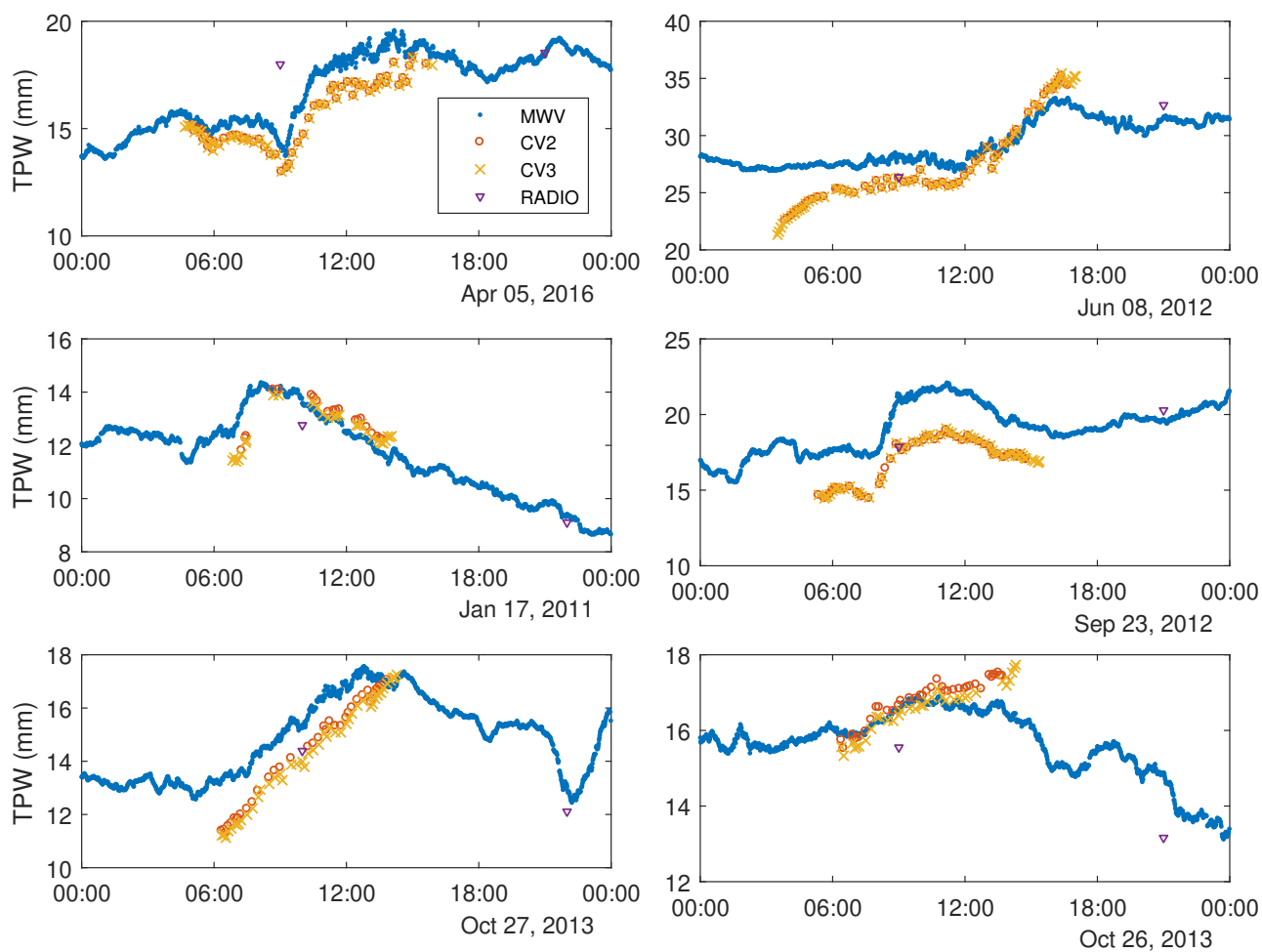
Figure 3. Diurnal variation of total precipitable water from radiosonde (magenta triangle), microwave radiometer (blue dots) and Cimel sun-photometer (V2 and V3 of the algorithm, red circle and green cross, respectively) for six randomly selected days (i.e., with a relative high number of Cimel measurements). The time is in UTC (i.e., local time + 2 hours).
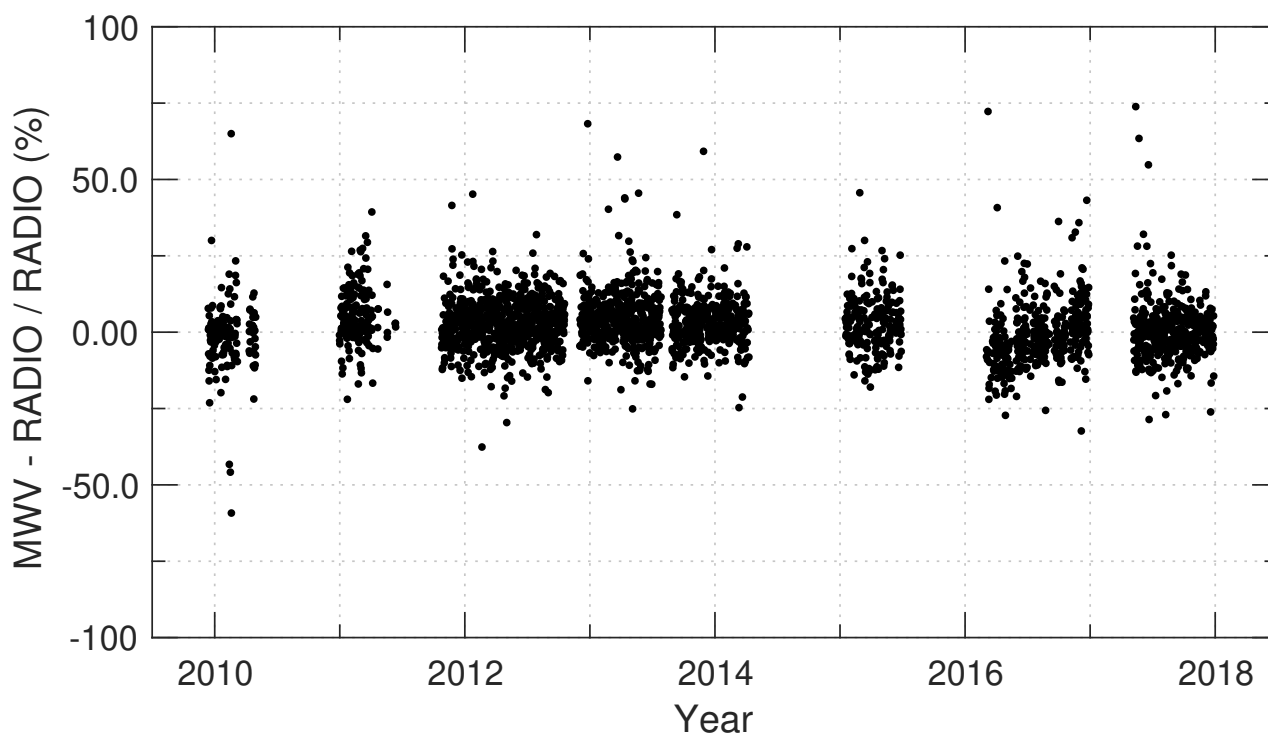
Figure 4. Time series of the relative difference (%) between the TPW from the microwave radiometer and the radiosonde during the period 2009—2017.
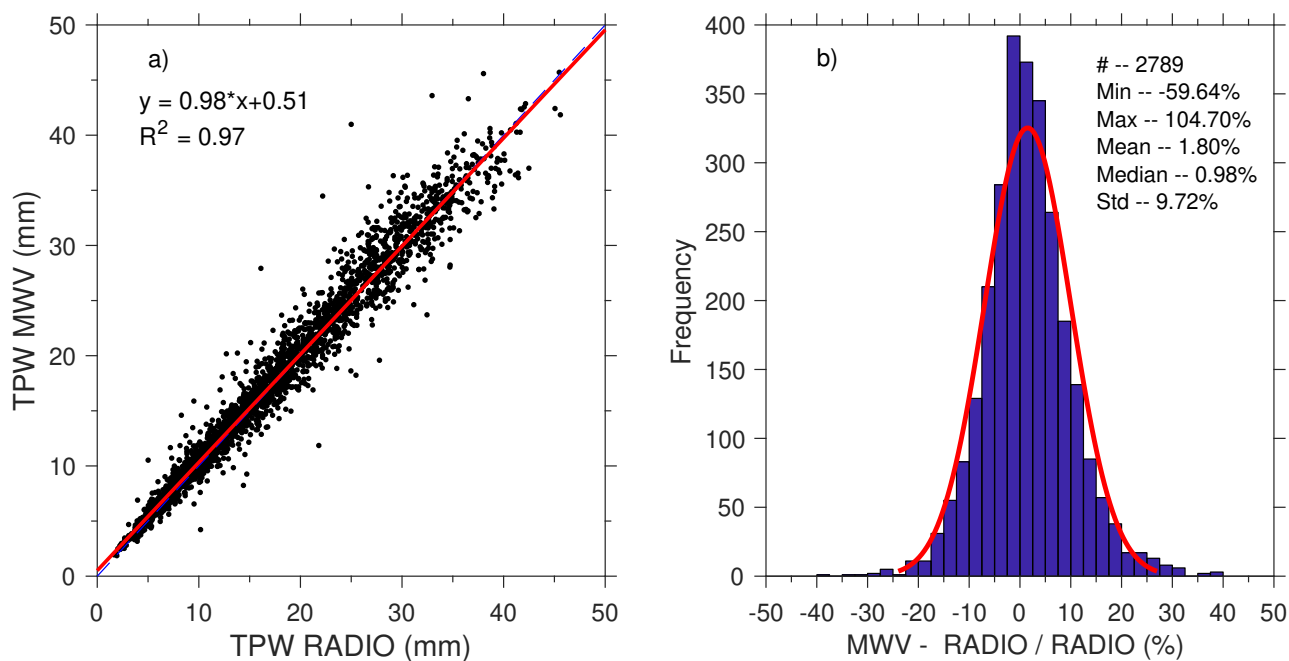
Figure 5. (a) Scatter plot of TPW values derived from microwave radiometer and radiosondes. The blue dashed line represents the identity line and the red solid line is the least square linear fit. (b) Frequency distribution of the relative mean difference in TPW between microwave radiometer and radiosondes in bins of 2.5% .
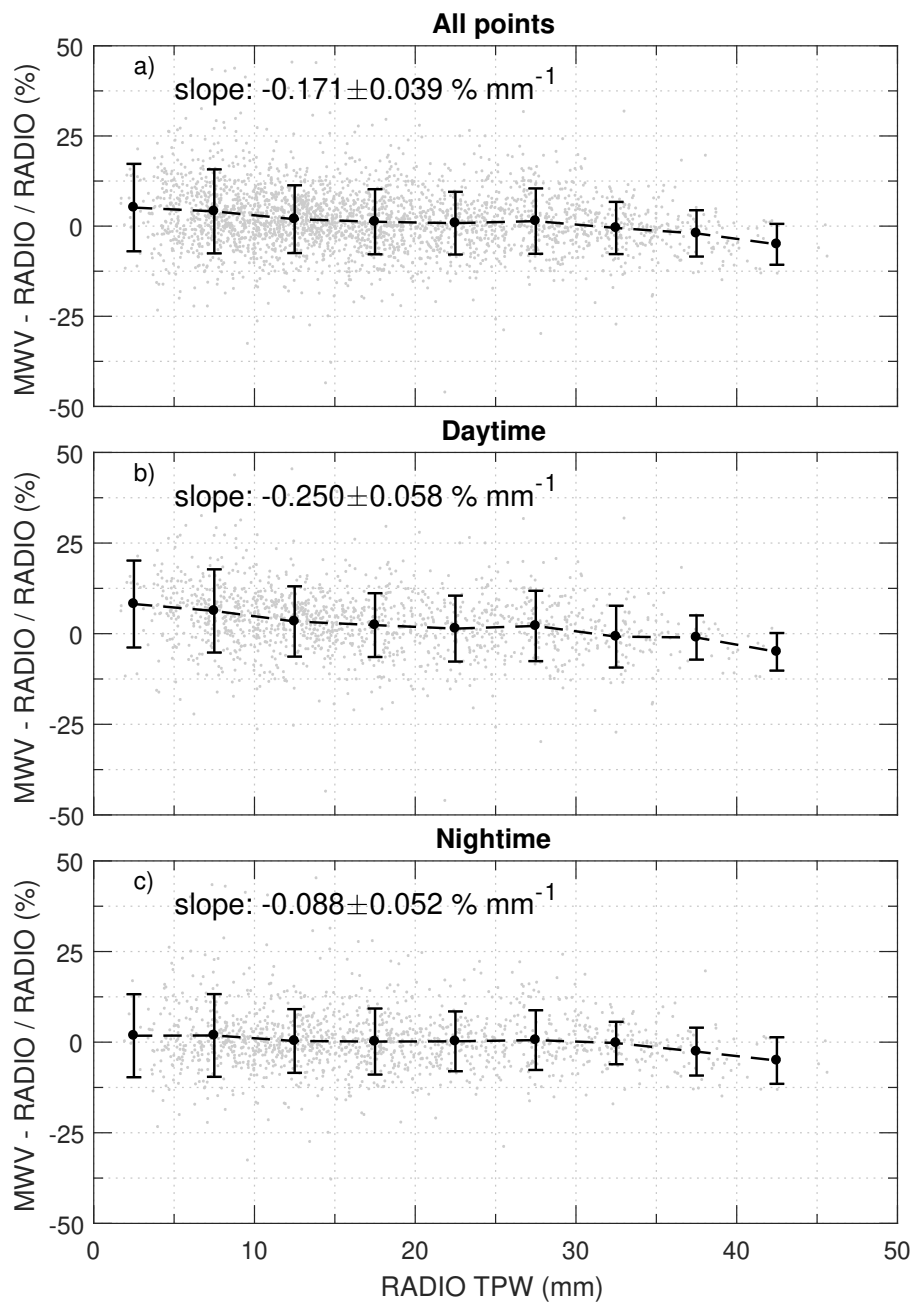
Figure 6. Dependence plot of the relative difference of the TPW from the microwave radiometer and the radiosondes from the total amount of TPW for (a) all points, (b) the daytime measurements, and (c) the nighttime measurements. The black dots show the average difference in bins of 5 mm and the error-bar represents their standard deviation. The linear fit is based on all measurements.
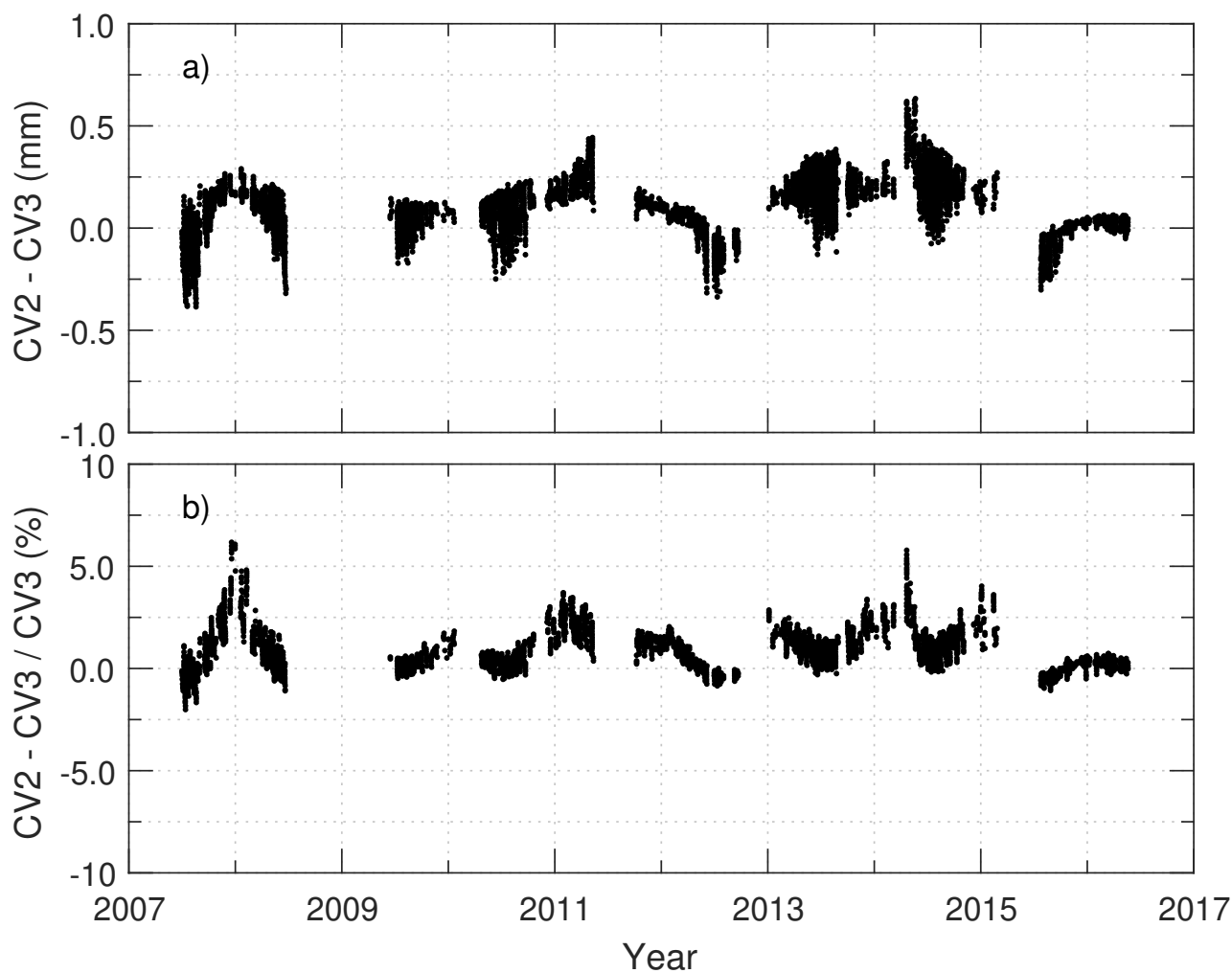
Figure 7. Time series of the (a) absolute and (b) relative differences between level 2.0 of V2 and V3 TPW from Cimel sun-photometer measurements, for their common measurements during the period 2007—2016.
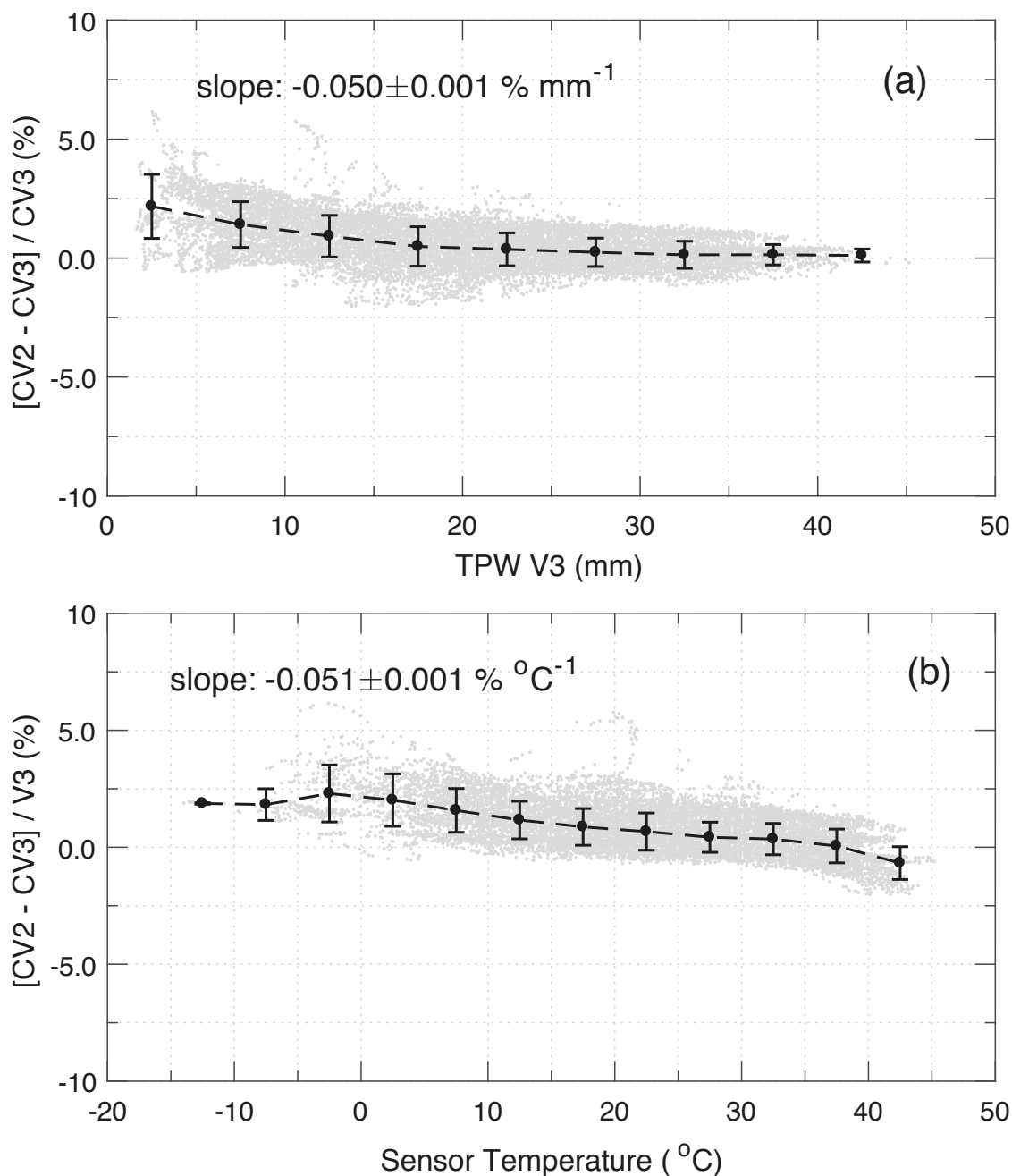
Figure 8. Dependence plot of the relative difference of the TPW from V2 and V3 AERONET algorithms from (a) the total amount of TPW and from (b) the temperature of the censor. The black dots show the average difference in bins of 5 mm and 5°C, respectively, and the error-bar represents the standard deviation of the mean. The linear fit is based on all measurements.
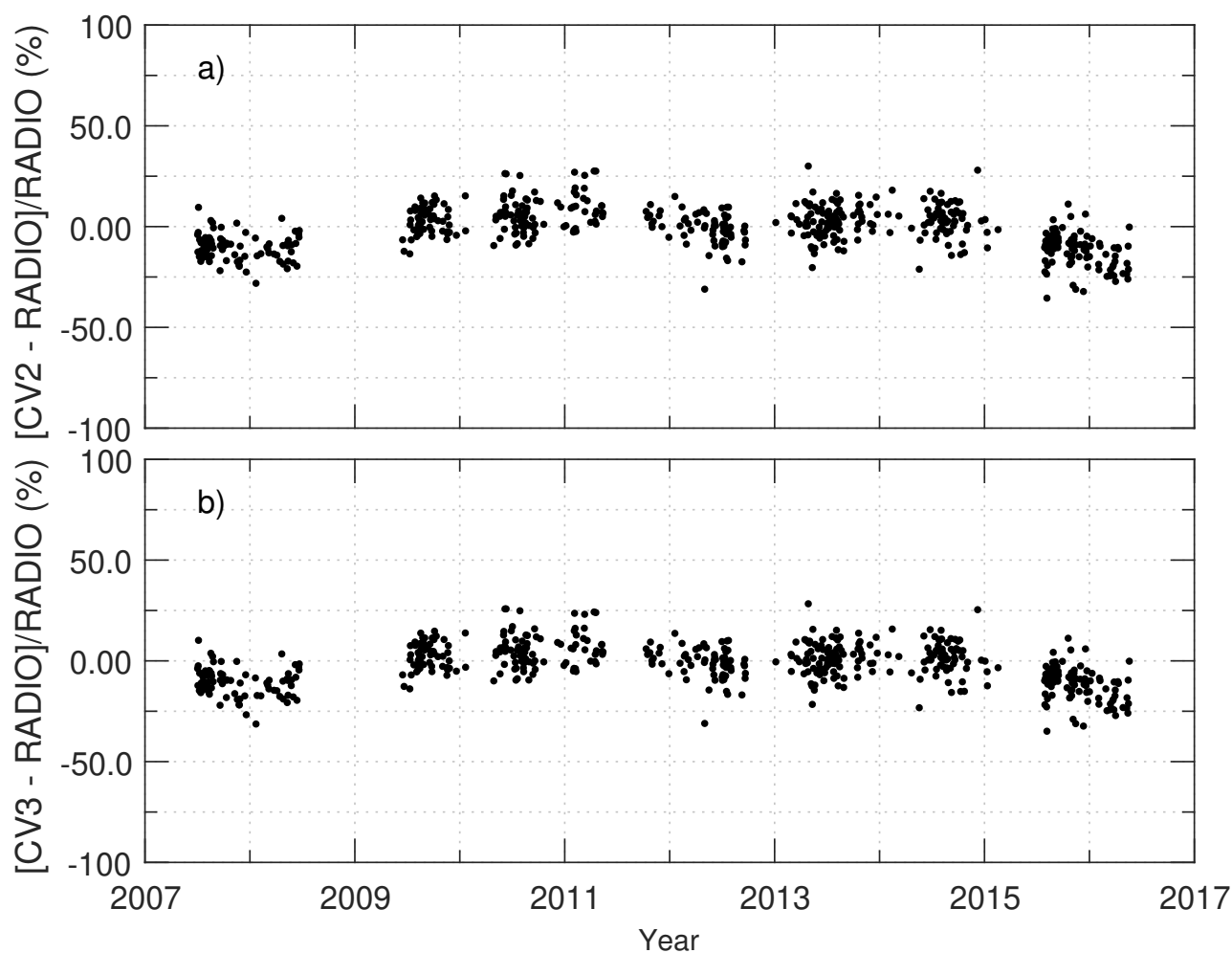
Figure 9. Time series of relative differences between (a) level 2.0 V2 TPW from Cimel sun-photometer and the radiosondes, and (b) from level 2.0 V3 TPW from Cimel, during the period 2007—2017.
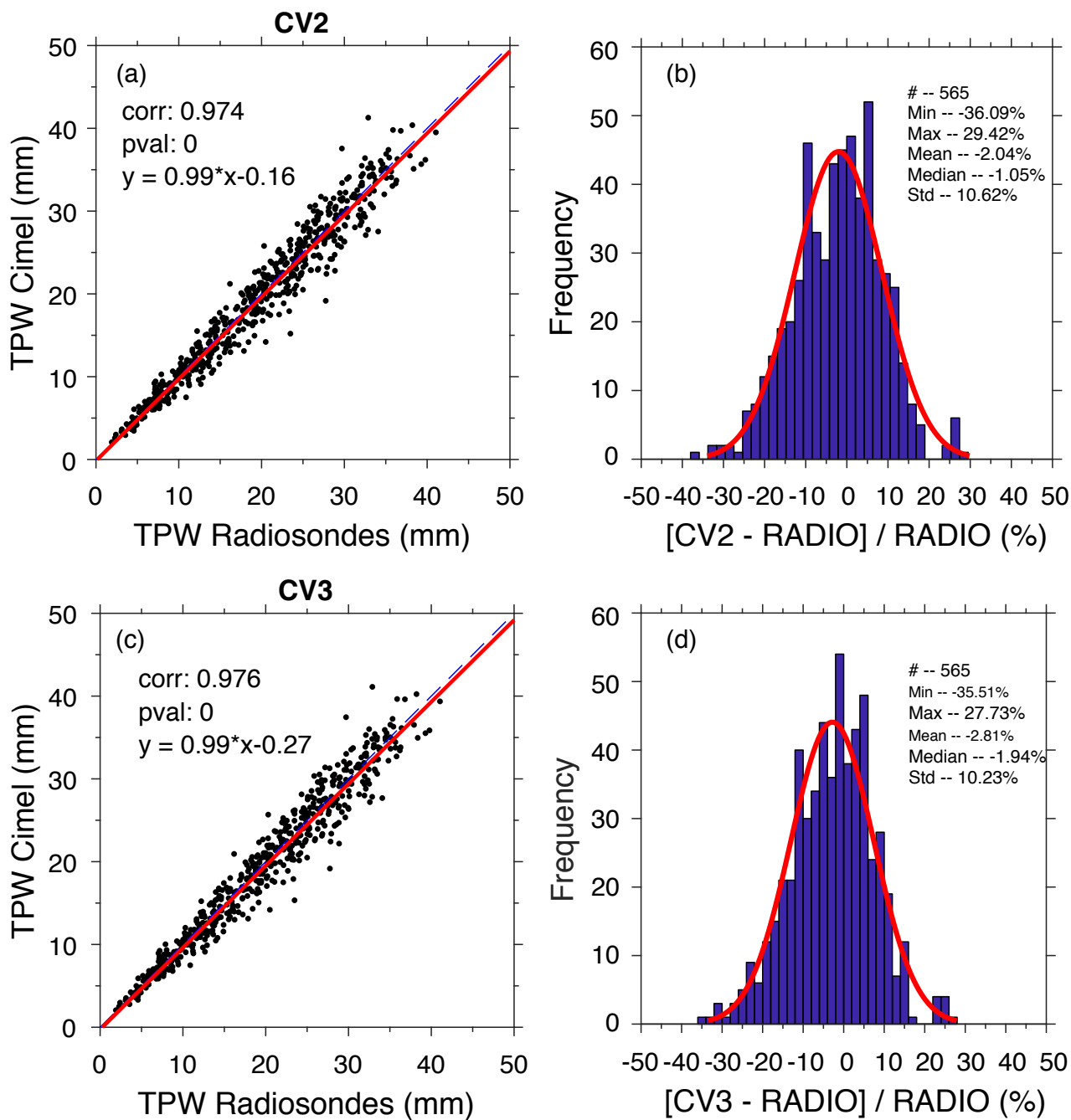
Figure 10. Scatter plot between the TPW from (a) the radiosondes-Cimel V2 and (c) Cimel V3. The red thick line shows the least square regression line and blue dashed line is the identity line. Frequency histogram of the relative difference between (b) the TPW from the radiosondes and CV2 and (d) CV3, respectively. The red line shows the fit of a normal distribution to the data.
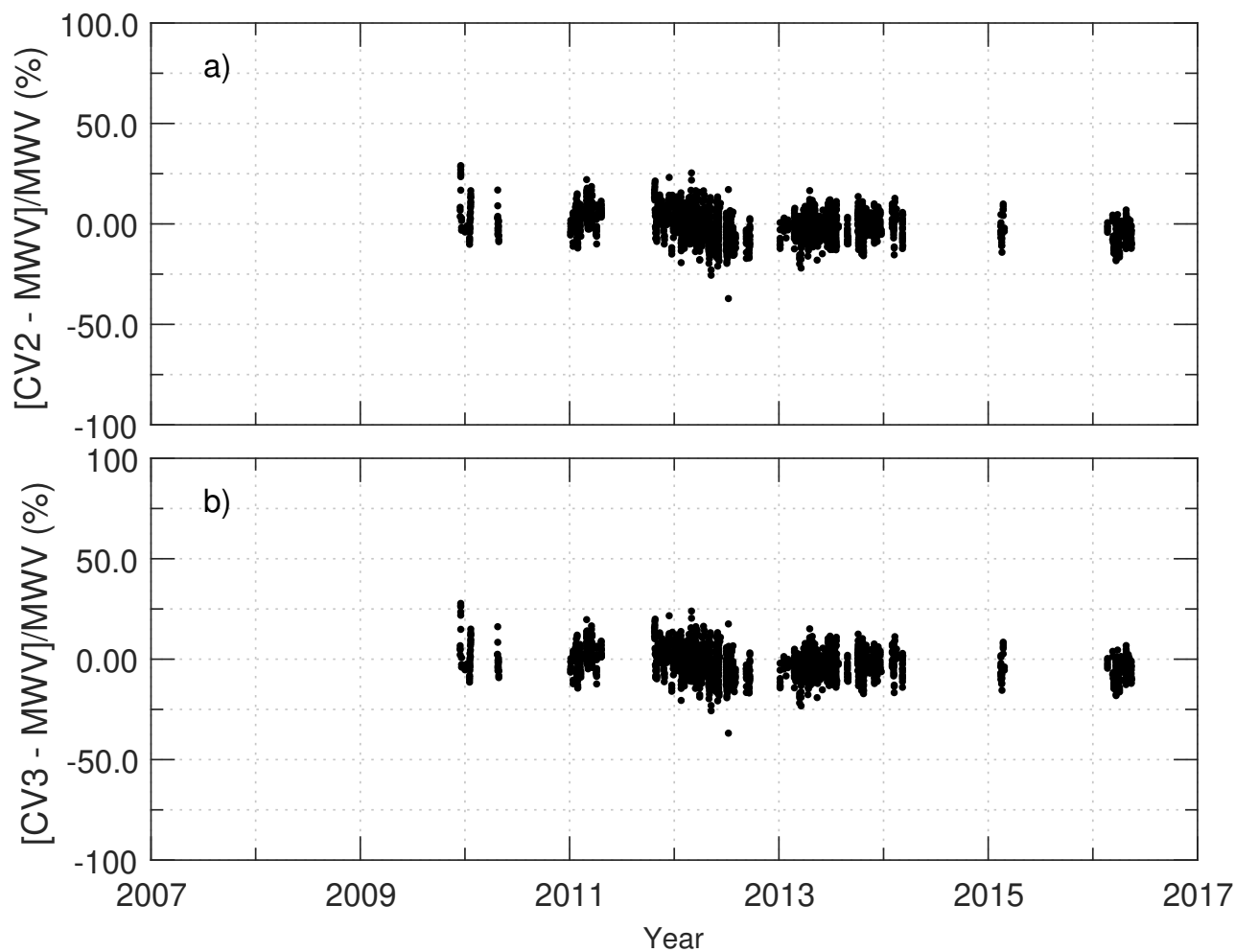
Figure 11. Time series of the relative differences between (a) level 2.0 V2 TPW from Cimel sun-photometer and the microwave radiometer, and from (b) level 2.0 V3 TPW from Cimel, during the period 2009-–2017.
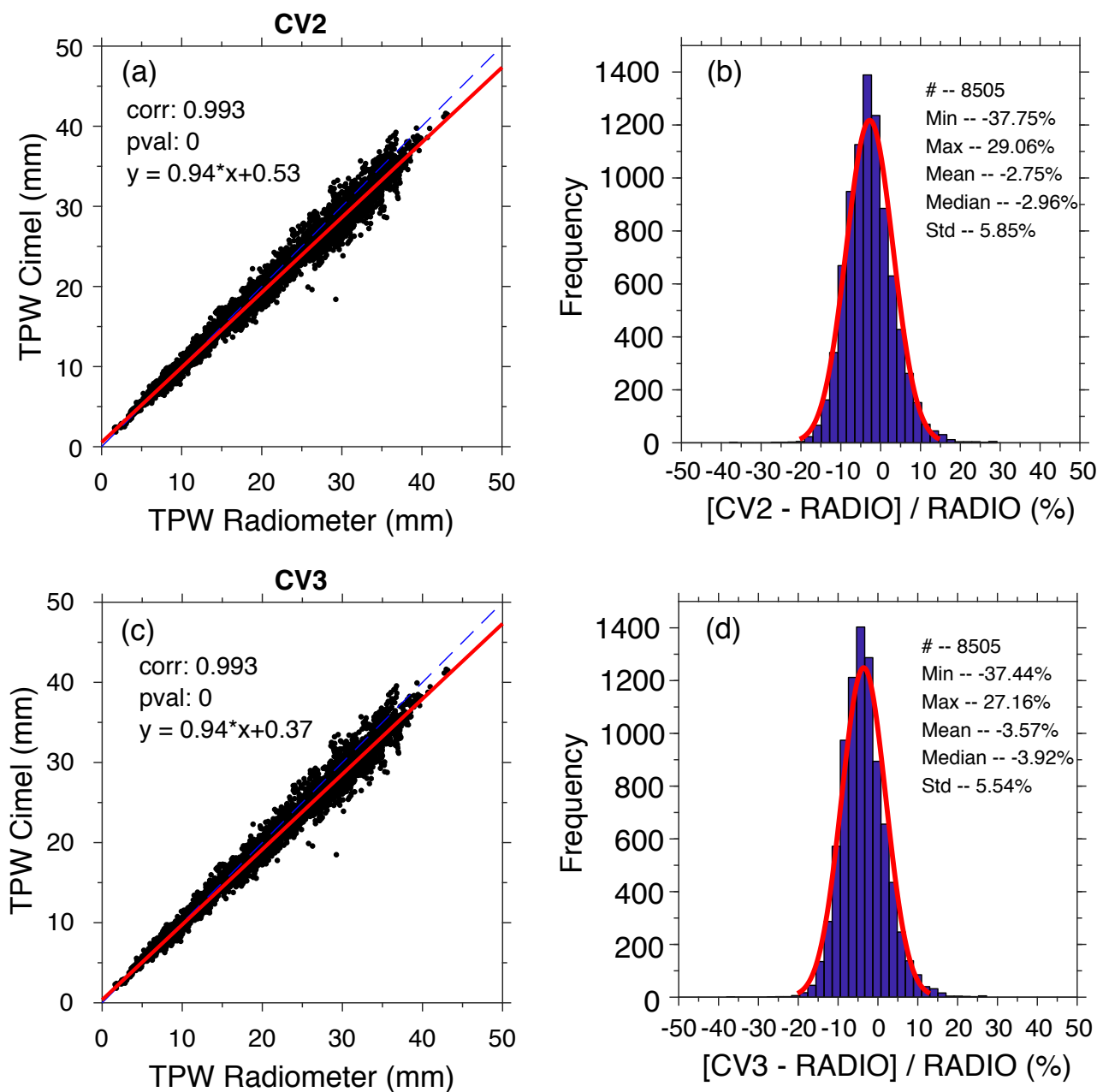
Figure 12. Scatter plot between the TPW from (a) the microwave radiometer-Cimel V2 and (c) Cimel V3. The red thick line shows the least square regression line and blue dashed line is the identity line. Frequency histogram of the relative difference between (b) the TPW from the microwave radiometer and CV2 and (d) CV3, respectively. The red line shows the fit of a normal distribution to the data.
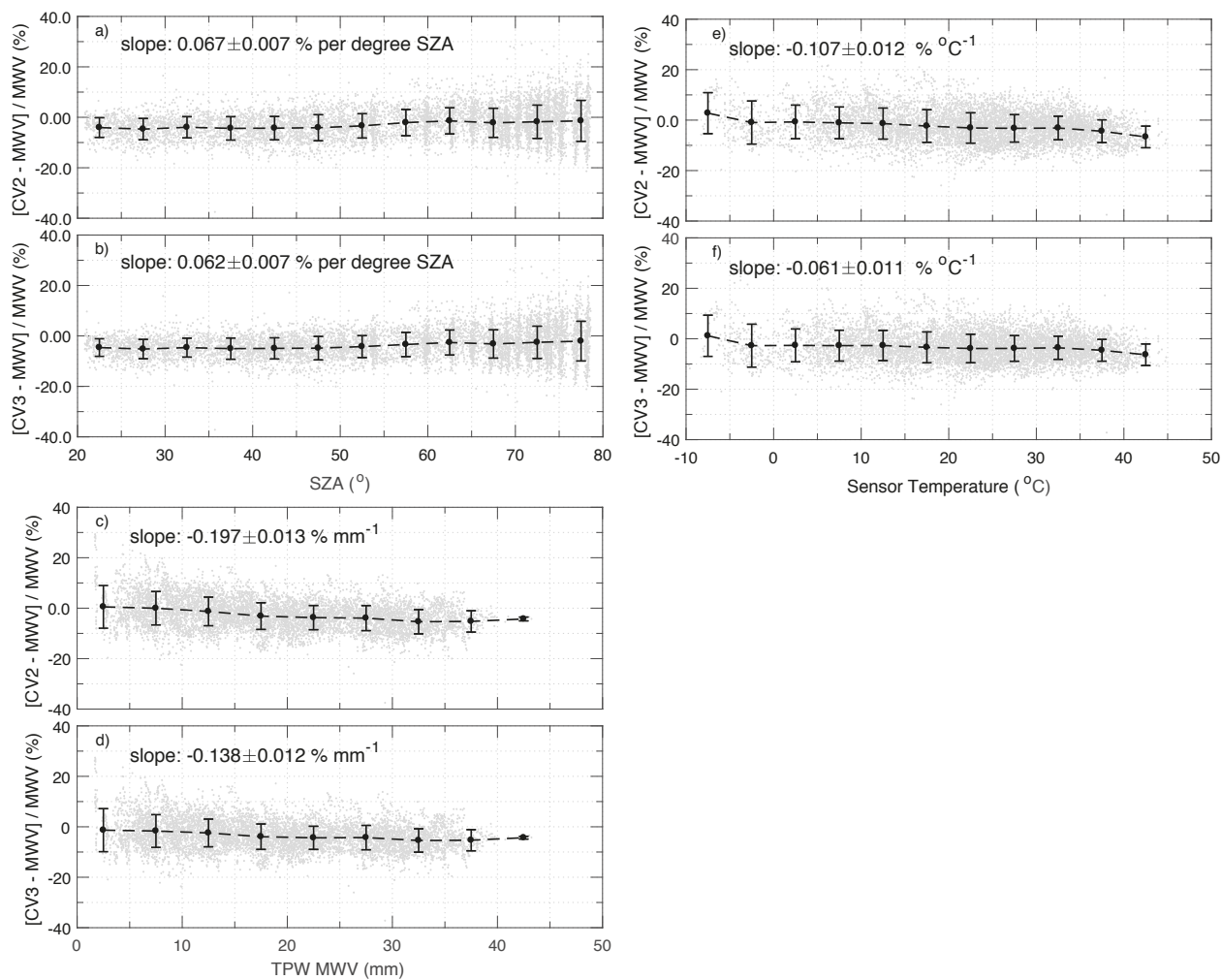
Figure 13. Dependence plot of the relative difference of the TPW from Cimel and the radiometer from the SZA (a) for Cimel V2 and (b) Cimel V3. The Relative between (c) Cimel V2 and (d) Cimel V3 as a function of TPW and the internal sensor temperature for (e) V2 and (f) V3. The black dots show the average difference in bins of 5 degrees, 5 mm and 5°C and the error-bar represents the standard deviation of the mean.

Table 1. Overview of the measurement characteristics and datasets used in this study for the period 2007—2017.

Instrument	Retrieval Method	Total number of observations	Total number of daily mean values	Data frequency
Radiosondes	Thin-film capacitance relative humidity sensors use of balloons for vertical profiles	7503	3784	12 hrs
Radiometer	Sky brightness temperature at 23.8GHz water vapor absorption band.	1859315	1612	2 sec
Cimel V2	Solar direct irradiance at 940nm absorption band	33324	1293	∼20 min for clear sky conditions
Cimel V3	Solar direct irradiance at 940nm absorption band	35373	1325	∼20 min for clear sky conditions

Table 2. Summary of intercomparison statistics for the period July 2007 to December 2017.

	Radiosondes	Radiometer	Cimel V2	Cimel V3
Average (mm)	18.75	17.47	18.86	18.58
Standard deviation (mm)	8.78	8.50	8.87	8.99
Maximum (mm) /(date)	43.48/(07.08.2017)	41.95/(07.08.2017)	41.27/(08.08.2010)	44.13/(16.07.2015)
Minimum (mm) /(date)	1.87/(01.02.2012)	2.04/(01.02.2012)	1.83/(01.02.2012)	1.83/(01.02.2012)

Table 3. Monthly mean and median values of TPW and their IQR from the different instruments used in this study.

Month	Radiosondes			Radiometer			Cimel V2			Cimel V3		
	mean	median	IQR	mean	median	IQR	mean	median	IQR	mean	median	IQR
January	9.69	9.12	5.65	10.40	10.39	5.83	7.27	6.62	4.99	7.66	6.98	5.53
February	10.09	10.14	6.28	10.20	10.12	5.98	9.04	9.10	6.79	8.99	8.35	6.03
March	11.42	11.04	5.94	11.49	10.87	5.71	10.05	9.40	5.37	9.81	9.17	5.00
April	15.17	15.18	6.27	15.54	15.74	6.03	14.03	14.20	4.50	13.94	14.00	4.90
May	20.92	20.69	7.63	21.73	21.98	7.43	19.69	19.41	7.33	19.36	19.16	6.43
June	27.23	27.58	7.47	28.58	28.70	6.64	26.47	26.84	7.89	26.36	26.91	7.94
July	29.64	29.67	8.11	29.78	30.45	6.88	27.82	27.91	8.32	28.28	28.20	8.05
August	28.95	29.44	8.25	28.11	29.05	8.60	27.75	27.77	7.50	27.71	27.77	7.64
September	23.32	22.87	9.55	22.36	22.06	7.43	20.71	20.35	7.05	21.41	20.86	7.37
October	18.30	18.38	9.59	18.79	17.86	8.24	15.41	14.47	9.06	15.28	14.49	8.25
November	14.37	13.95	7.47	14.15	13.71	6.39	12.00	11.13	6.27	11.65	10.75	6.13
December	10.62	9.83	6.41	10.65	10.06	5.54	9.23	9.00	5.88	9.49	9.14	6.04